Bioconjugate Chemistry

Article

pubs.acs.org/bc

Peptide-Nanoparticle Ligation Mediated by *Cutinase* Fusion for the Development of Cancer Cell-Targeted Nanoconjugates

Elisabetta Galbiati,[†] Marco Cassani,[†] Paolo Verderio,[‡] Enzo Martegani,[†] Miriam Colombo,[†] Paolo Tortora,[†] Serena Mazzucchelli,*[,§] and Davide Prosperi*[,†]

[†]Dipartimento di Biotecnologie e Bioscienze, Università di Milano-Bicocca, Piazza della Scienza 2, 20126 Milano, Italy

[‡]Nerviano Medical Sciences s.r.l., viale Pasteur 10, 20014 Nerviano (MI), Italy

[§]Dipartimento di Scienze Biomediche e Cliniche "Luigi Sacco", Università di Milano, Ospedale L. Sacco, via G.B. Grassi 74, 20157 Milano, Italy

Supporting Information

ABSTRACT: The relationship between the positioning of ligands on the surface of nanoparticles and the structural features of nanoconjugates has been underestimated for a long time, albeit of primary importance to promote specific biological recognition at the nanoscale. In particular, it has been formerly observed that a proper molecular orientation can play a crucial role, first optimizing ligand immobilization onto the nanoparticles and, second, improving the targeting efficiency of the nanoconjugates. In this work, we present a novel strategy to afford peptide-oriented ligation using genetically modified *cutinase* fusion proteins, which combines the presence of a site-directed "capture" module based on an enzymatic unit and a "targeting" moiety consisting of the ligand terminal end of a genetically encoded polypeptide chain. As an example, the oriented presentation of U11 peptide, a sequence specific for the recognition of urokinase plasminogen activator receptor (uPAR), was achieved by enzyme-mediated conjugation with an irreversible inhibitor of cutinase, an alkylphosphonate *p*-nitrophenol ester linker, covalently bound to the surface of iron oxide nanoparticles. The targeting efficiency of the resulting protein−nanoparticle conjugates was assessed using uPAR-positive breast cancer cells exploiting confocal laser scanning microscopy and quantitative fluorescence analysis of confocal images. Ultrastructural analysis of transmission electron micrographs provided evidence of a receptor-mediated pathway of endocytosis. Our results showed that, despite the small average number of targeting peptides presented on the nanoparticles, our ligand-oriented nanoconjugates proved to be very effective in selectively binding to uPAR and in promoting the uptake in uPAR-positive cancer cells.

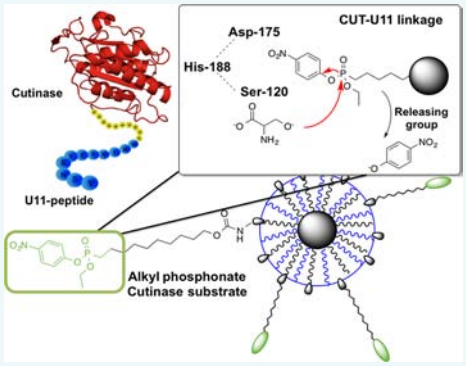

INTRODUCTION

Colloidal nanoparticles can be designed to achieve an excellent targeting efficiency toward specific molecular receptors in malignant cells and tissues.[1−3] To reach this goal, they need to be functionalized with appropriate homing ligands.[4−6] When short peptides are selected as targeting ligands, they have to be tightly anchored to the nanoparticle surface and at the same time sufficiently flexible in order to interact predominantly with their molecular target.[7−9] However, the capability of ligand-conjugated colloidal nanoparticles to recognize a receptor is a complex challenge to be considered carefully. According to this, more recent and advanced studies take advantage of different strategies to achieve a controlled orientation of ligands on the nanoparticle surface.[8,10] Indeed, the ligand/peptide positioning on the surface determines the bioactivity, the avidity, and the targeting efficiency of the functionalized nanoparticles.[7] Therefore, the possibility to control the ligand orientation after nanoparticle conjugation is a fundamental step to optimize the receptor recognition.[11−13] These methods have indeed brought the "orientation issue" to the attention of nanobiotechnology. Among colloidal nanoparticles, multifunctional iron oxide nanoparticles (MNP) showed a great promise for the development of noninvasive tools for the diagnosis and treatment of malignant diseases.[14,15] Thus, in order to optimize the targeting efficiency of MNP for biomedical applications, it is of primary importance that targeted molecules are immobilized in an oriented way.[16,17]

Recently, we have explored a novel "bimodular ligation" strategy to achieve a well-oriented presentation of peptides on nanoconjugates. This approach involves a fusion protein as a ligation unit containing both a "capture" and a "targeting" module (Figure 1). While the targeting module is a protein or a peptide that selectively recognizes the specific receptor overexpressed on the plasma membrane of cancer cells, the capture unit is a genetically encoded small enzyme capable of a covalent, selective, and irreversible cross-coupling with a suicide

Received: January 5, 2015
Revised: March 4, 2015
Published: March 5, 2015

DOI: 10.1021/acs.bioconjchem.5b00005
Bioconjugate Chem. 2015, 26, 680−689

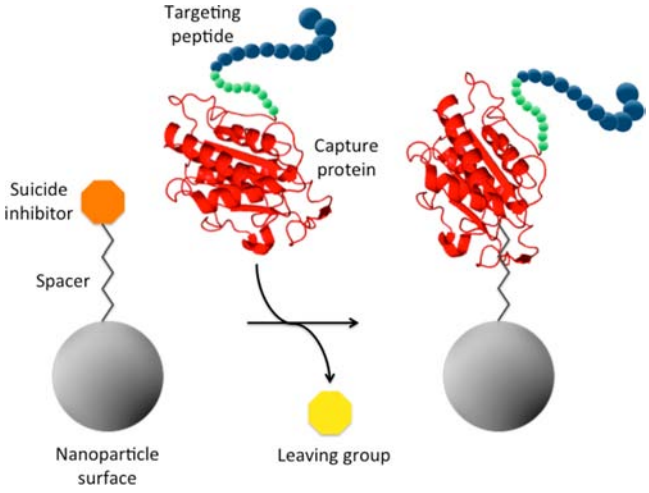

Figure 1. Schematic strategy adopted for the oriented conjugation of peptides. The peptide of interest is genetically fused with a capture protein, which specifically binds to a suicide inhibitor anchored onto a colloidal nanoparticle. This enzymatic reaction results in a covalent immobilization of a peptide that maintains its activity and accessibility.

inhibitor anchored to the nanoparticle surface. In a few examples, this approach was proven to optimize the orientation-controlled display of the peptide in MNP exploiting an enzymatic conjugation without any artificial chemical reaction.[18,19] Moreover, the ligand of biological interest is always oriented in the correct way due to the natural folding of the fusion protein.[20,21] We have previously demonstrated that the functionalization of MNP with short peptides via the bimodular ligation strongly improves both affinity and selectivity toward specific cell membrane receptors when a small number of ligands is presented.[21] Several advantageous features can be envisaged using the bimodular ligation, including (1) the protein attachment to the nanoparticle occurs via a single ligation event in a site-directed manner exploiting the enzyme binding pocket, which results in a proper orientation that allows the maximal protein functionality; (2) the nature of the enzymatic ligation is highly specific and irreversible and also occurs under physiological conditions thus preventing protein degradation or denaturation;[22] (3) the immobilized linker is a small molecule, which reduces the overall nanoparticle size; (4) this strategy is applicable to a wide range of target proteins, which can be (genetically) engineered in order to introduce a specific sequence for protein immobilization.[23] Recently, two engineered capture proteins genetically fused with a targeting peptide have been adopted for MNP functionalization, namely, O_6-alkylguanine-DNA transferase (SNAP tag) and haloalkane dehalogenase (HALO tag). These two modified enzymes were fused with an anti-HER2 scFv antibody and with a small 11-amino-acid peptide (U11), respectively.[20,21,24]

In this paper, we extend the potential of the bimodular ligation investigating cutinase (CUT) from *Fusarium solani pisi* as a capture component. CUT is a 22 kDa serine esterase that forms a site-specific covalent adduct with a phosphonate ester ligand, which mimics the tetrahedral transition state of an ester hydrolysis. The phosphonate ester is attacked by the catalytic Ser120 residue of the enzyme, resulting in the displacement of a leaving group with subsequent formation of a stable covalent adduct that is indeed resistant to hydrolysis (Figure 2).[22] Moreover, the enzyme is small, globular, and monomeric, all features that minimize the steric hindrance of the fused peptides. Due to the excellent propensity of *p*-nitrophenol to play the role of a living group in nucleophilic addition, we reasoned that an alkylphosphonate *p*-nitrophenol ester linker could be a good candidate to mediate the covalent, oriented immobilization of a homing peptide genetically fused with CUT on the MNP. We designed a modular genetic fusion of CUT (CUT−U11) comprising a small peptide of 11 amino acids (U11) that has high affinity toward the urokinase plasminogen activator receptor (uPAR), a glycoprotein tethered to the cell membrane through a glycosylphosphatidylinositol (GPI) anchor.[25,26] This protein has been identified as a possible target in cancer research, as it is found overexpressed in several metastasizing breast and prostate cancers and its overexpression is generally related to a poor prognosis.[27] Unfortunately, the efficiency of U11 nanoconjugates in which the peptide is directly linked to the surface of colloidal nanoparticles is substantially reduced compared to the free molecule, because, when the peptide density is high, U11 undergoes self-assembly into β-sheets that are almost completely inert toward uPAR resulting in a nanoparticle aggregation.[28]

In the present work, CUT−U11 was produced in *E. coli* and reacted quickly, effectively, and in a site-directed manner with an alkylphosphonate *p*-nitrophenol ester derivative immobilized on MNP. The targeting efficiency of the resulting U11-functionalized MNP against uPAR-positive breast cancer cells has been assessed by confocal laser scanning microscopy and

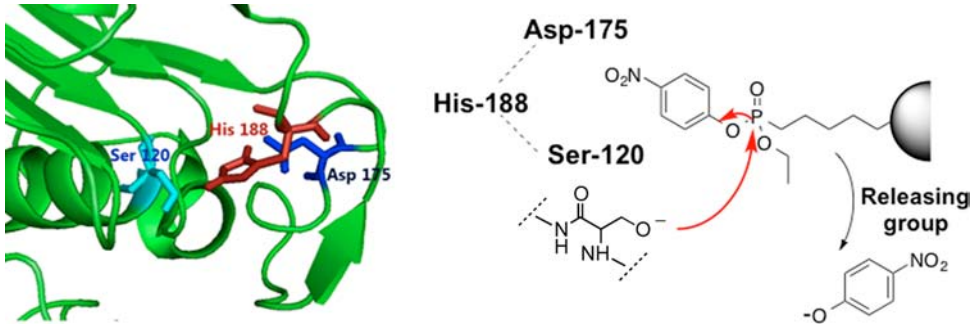

Figure 2. Schematic view of the bioorthogonal enzymatic reaction between the engineered CUT−U11 protein and the alkylphosphonate *p*-nitrophenol ester derivative exposed from the nanoparticle surface. Each enzyme is small and globular and contains a single catalytic site: these characteristics minimize all steric effects. The phosphonate group, which mimics the tetrahedral transition state of an ester hydrolysis, is attacked by the catalytic serine (Ser-120) residue, resulting in the displacement of the leaving group and formation of a stable covalent adduct.[29,30]

DOI: 10.1021/acs.bioconjchem.5b00005
Bioconjugate Chem. 2015, 26, 680−689

quantified by measurements of the fluorescence emission from analyzed cells in confocal images.

RESULTS AND DISCUSSION

Magnetite nanoparticles (MNP0) with a narrow size distribution (7.41 ± 1.1 nm by transmission electron microscopy, TEM, Figure S1) capped with oleate surfactant were obtained by solvothermal decomposition in octadecene.[31] MNP0 were transferred to the water phase by coating them with an amphiphilic polymer, termed PMA,[32] in sodium borate buffer (SBB) at pH 12, following a procedure described previously.[33] The resulting PMA-coated nanoparticles (MNP1) were functionalized with amino groups by using a *bis*-amino homobifunctional linker, the 2,2-(ethylenedioxy)bis-(ethylamine) (EDBE), to achieve MNP2. Then, the alkyl phosphonate L1 was linked to the amines on the PMA envelope by nucleophilic addition to the carbonyl imidazole group at 4 °C (Scheme 1).

Although these nanoparticles were not pegylated, they were highly soluble thanks to the effect of CUT favorably affecting colloidal stability and exhibited very low tendency to aggregate (see Figure S2). Alternatively, to obtain fluorescent nanoparticles, PMA was labeled with FITC prior to the reaction with MNP0, giving MFP1. Both MNP1 and MFP1 displayed good monodispersity in size and excellent colloidal stability for months. The nanoparticles were characterized by dynamic light scattering (MNP1, DLS size = 21.1 ± 1.6 nm in 1 mM NaCl pH 7.2) and ζ potential (−45.3 ± 5.6 mV). Table S1 in the Supporting Information summarizes the DLS characterization data.

CUT enzyme was produced in *E. coli* strain Origami-(DE)-RIL/pET-11a/CUT (see Experimental section and Figure S3) with a final yield of 1.34 mg L^{-1} of culture medium. The presence of the protein was assessed by sodium dodecyl sulfate polyacrylamide gel electrophoresis (SDS-PAGE, Figure S4) and Western blot analysis using a His-Tag probe (Figure S5). The molecular weight of the most pronounced band in SDS-PAGE corresponded to the molecular weight of CUT. In parallel, the CUT−U11 fusion was expressed in Tuner(DE3) *E. coli* strain in 1.0 mg L^{-1} yield. Due to the lower purification yield compared to CUT, we concluded that the presence of U11 peptide could play a critical role in destabilizing the enzyme. Also, in this case, the presence of the protein was verified by SDS-PAGE (Figure S7) and Western blot analysis using an anti-His-tag antibody (Figure S8). Although the analysis showed impurities in all fractions, the presence of the desired protein was clearly confirmed as a band around 25 kDa.

Bioconjugation was carried out in a 1:2 fixed weight ratio between MNP3 and CUT−U11. Three different amounts of MNP3/CUT−U11, 25:50 (1), 50:100 (2) and 125:250 (3) μg, were reacted for 1 h at room temperature. All the reactions were performed using fluorescent CUT−U11, with the purpose to quantify spectrofluorometrically the amount of protein immobilized on the nanoparticles. A standard calibration curve based on a dye-labeled CUT−U11 (CUT−U11−FITC) was determined (Figure S10). The nanoparticles from the reaction mixtures were centrifuged, washed three times, and resuspended in phosphate buffer saline (PBS), pH 7.4. The amount of immobilized protein in each batch was quantified by interpolating the intensity of fluorescence of the sample with the above standard calibration curve (Figure S11 and Table S3). The highest amount of immobilized protein was measured under the third condition tested. Hence, we decided to standardize all further experiments with a MNP3 to CUT−U11 ratio corresponding to 125 μg of MNP3 per 250 μg of protein.

Scheme 1. Schematic Representation of the Synthesis of MNP−C11 (and MFP−C11)[a]

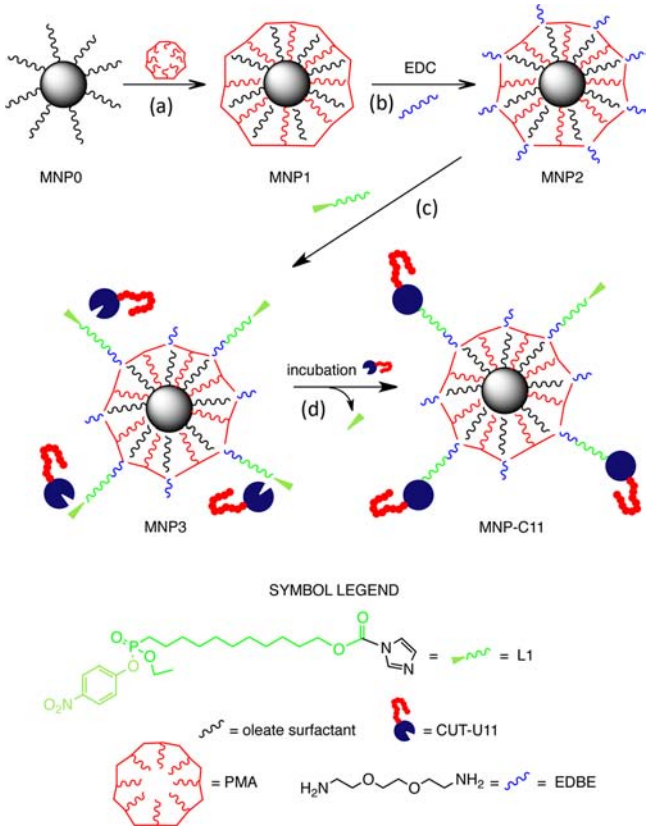

[a]Iron oxide nanocrystals coated by oleic acid (MNP0) were transferred to water phase by using the amphiphilic polymer PMA, which was able to intercalate its hydrophobic chains between the oleic acid chains leading to a tight hydrophobic interaction. At the same time, the hydrophilic carboxylate groups deriving from maleimide rings were exposed to the solvent. (a) The phase transfer of MNP0 was conducted in SBB, pH 12 (MNP1). (b) Amino functionalities were introduced by amide coupling, mediated by EDC, between the carboxylic groups of the polymer and amino groups of the homobifunctional spacer EDBE (MNP2). (c) Addition of L1 to MNP2 gave the conjugate MNP3. (d) The incubation with CUT resulted in MNP-C, while the reaction with CUT-U11 led to MNP−C11. When fluorescent PMA (PMA-FITC) was used, the corresponding MFP1, MFP2, MFP3, MFP−C, and MFP−C11 were obtained, respectively. DLS data of MNP−C and MNP−C11 were consistent with a stable colloidal dispersion of nanoparticles in biocompatible media (see Figure S2).

To evaluate the specificity of the conjugation reaction, two different approaches were followed. First, MNP1 or MNP3 was incubated with CUT−U11 in a 1:2 ratio ($w_{NP}/w_{protein}$). After incubation, the reactions were stopped removing the unreacted protein by centrifugation through Amicon YM-100 filters. The residual enzymatic activity of the immobilized CUT−U11 was determined in nanoconjugates to assess whether the bond between the enzyme and the nanoparticle was exclusively mediated by L1 or passive adsorption was also present and to what extent. In this experiment, 4-nitrophenyl decanoate was used as a substrate to quantify CUT−U11 activity. If a specific conjugation took place via covalent reaction with L1, the resulting immobilized enzyme should have been irreversibly

DOI: 10.1021/acs.bioconjchem.5b00005
Bioconjugate Chem. 2015, 26, 680−689

inhibited, as the phosphonate linked to MNP3 would have competed with the substrate for the active site of the enzyme. In accordance with our expectations, Figure 3 shows that

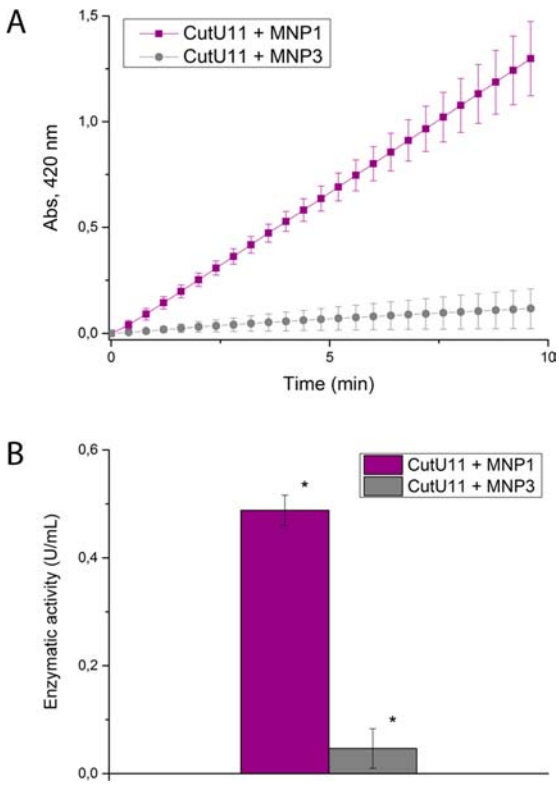

Figure 3. Enzymatic activity of CUT−U11 immobilized on nanoparticles functionalized with L1 (MNP3, gray circles) or not (MNP1, purple squares), expressed (A) in absorbance values at 420 nm as a function of the incubation time and (B) in enzymatic units (U) after 5 min incubation. Data are expressed as means ± standard deviation (SD) of 3 independent experiments. $P < 0.05$.

CUT−U11 maintained linear activity when incubated with nanoparticles lacking the reactive ligand L1 (MNP1), while MNP3 displayed a much lower activity compared to MNP1, which further declined at longer incubation times.

Therefore, the very low esterase activity of CUT−U11 reacted with MNP3 compared to that observed with CUT−U11 reacted with MNP1 provides evidence in support of the hypothesis that the fusion protein was predominantly immobilized via a covalent bond with the phosponate linker. However, we observed a residual amount of enzyme that seemed to be nonspecifically adsorbed to the nanoparticles.

In a second experiment, CUT−U11 was reacted with its inhibitor, 4-nitrophenyl phosphonate, resulting in the inhibited enzyme (CUT−U11−I), and, after removing the excess of unbound inhibitor, was incubated with MNP3. Unbound protein was recovered at the end of the conjugation reaction by centrifugation in Amicon YM-100 tubes, and then MNP−C11 were washed 3 times with PBS. The total protein content (excluded wash volume) was assessed by Bradford assay. Surprisingly, we observed that about 91% of CUT−U11−I was bound to the nanoparticles, suggesting that a nonspecific adsorption of CUT−U11 to the MNP surface occurred even in the absence of a binding event. In addition, as mentioned above, MNP1 was also able to nonspecifically bind CUT−U11. The overall protein content was analyzed by Bradford assay after washing 3 times the nanoparticle suspension, showing, in this case, that 63% of protein was nonspecifically adsorbed. Considering that a huge nonspecific adsorption could not be prevented unless with nanoparticle surface modification, we worked to ameliorate the specific binding of CUT−U11 to the nanoparticles by using different approaches.

In a first attempt, MNP−C11 was incubated in PBS supplemented with SDS following a previously published procedure.[22] This method proved inefficient in our hands, since a white precipitate at the bottom of the tube after centrifugation was recovered, probably due to the PMA coating detachment from the nanoparticle surface. Moreover, under these conditions, the protein quantification was not feasible. A second strategy was accomplished altering the ionic strength of the reaction mixture. Since all of the above-mentioned MNP intrinsically exhibit a strong net negative charge and isoelectric points of CUT and CUT−U11 are 7.89 and 8.37, respectively, we hypothesized that washing nanoparticles at pH above these IP values would mitigate the nonspecific protein adsorption. However, this approach did not yield the expected outcome either.

In a third chance, we decided to saturate all possible nonspecific binding area on the nanoparticle surface by using a medium supplemented with bovine serum albumin (BSA). We reasoned that the BSA adsorption on nanoparticles could prevent the nonspecific interaction with CUT, thus allowing CUT to freely react with MNP3 only through its specific alkyl phosphonate substrate. This effect is reminiscent of the spontaneous adsorption of plasma protein on nanoparticles forming the so-called "protein corona". In this assay, CUT−U11−FITC was used to quantify spectrofluorometrically the amount of conjugated proteins on MNP. Before bioconjugation with CUT−U11−FITC, MNP3 were incubated in PBS buffer supplemented with 0.3 wt % BSA and washed twice in PBS by centrifuging 30 min at 17000 *g*. A control mix was set using MNP1. The supernatant was discarded, MNP−C11−FITC were resuspended in PBS once again, and their fluorescence was measured. The fluorescence intensity was 10-fold higher in MNP3 than in MNP1 incubated with CUT−U11−FITC (see Figure 4).

A yellow pellet was detectable upon centrifugation of MNP3 after incubation with BSA followed by CUT−U11−FITC, due to the presence of dye. In contrast, the pellet obtained after reaction of CUT−U11−FITC with MNP1 was dark. This result accounted for a specific reaction of the enzyme with the alkyl phosphonate linker on MNP3. The amount of immobilized protein was quantified fluorometrically by comparison with a calibration curve of CUT−U11−FITC in the same buffer (Figure S10). This method allowed us to estimate 4 CUT−U11−FITC molecules per MNP3 and 1 protein molecule nonspecifically adsorbed on MNP1.

Data from DLS and ζ-potential of MNP−C11 substantiated these results. The hydrodynamic diameter increased from 31.7 ± 2.4 nm in MNP3 to 36.9 ± 2.3 nm in MNP−C11 due to the protein binding. The different sizes recorded for MNP−C (34.6 ± 1.8 nm) and MNP−C11 could be attributed to the presence of U11 peptide that enhanced the hydration sphere of nanoparticles. ζ-Potential measurements showed a remarkable decrease in the surface charge of MNP3, which changed from −65.3 ± 7.2 mV to −45.8 ± 3.4 mV in MNP−C11 and −51.01 ± 5.6 in MNP−C. In addition, the lower negative charge of MNP−C11 could be attributed to the presence of U11, which bears a positive charge.

DOI: 10.1021/acs.bioconjchem.5b00005
Bioconjugate Chem. 2015, 26, 680−689

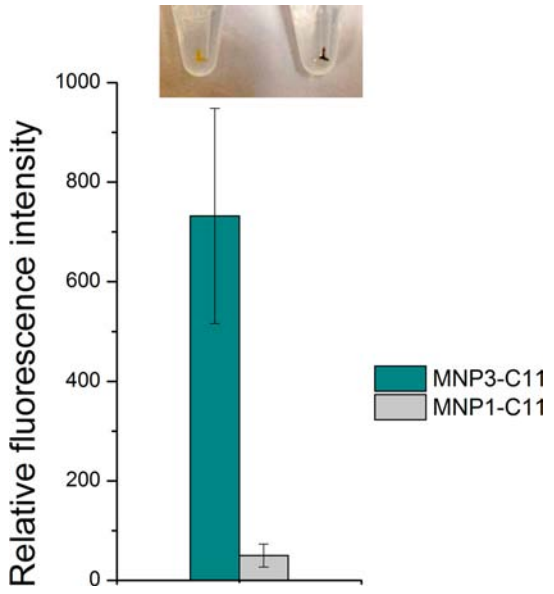

Figure 4. Relative fluorescence intensity of CUT−U11−FITC immobilized on MNP1 (gray) and on MNP3 (cyan). Inset: tubes containing CUT−U11−FITC reacted with MNP3 (yellow pellet) and with MNP1 (black pellet). Data are expressed as means ± SD of three independent experiments.

Once the conjugation of CUT−U11 to MNP3 was optimized, magnetofluorescent nanoparticles (MFP−C11), obtained by reacting FITC-labeled MNP3 (MFP3) with CUT−U11, were developed to test the biological activity of nanoconjugated U11 in MDA-MB-468 uPAR-positive cells. MFP−C were tested as negative control of U11 specificity toward uPAR-positive cells. MFP−C11 and MFP−C (100 μg mL^{-1}) were incubated in culture medium with MDA-MB-468 cells for 1 h at 37 °C. As expected, MFP−C11 was localized on MDA-MB-468 cell membrane and inside the cytoplasm, as a consequence of their internalization (Figure 5). In contrast, MFP−C did not show any fluorescence in proximity of the cells. These findings, combined with the results obtained by quantification of MFP fluorescence intensity throughout the acquired images, confirmed the targeting capability of MFP−C11 and suggested that this recognition was mediated by specific U11/uPAR interaction. To exclude a possible involvement of BSA adsorbed on MFP−C11 in the cell recognition, MDA-MB-468 cells were treated with BSA-coated MFP3 under the above conditions. The analysis of confocal images shows that nanoparticles were not significantly uptaken by MDA cells at the considered time points (Figure S12). CAL-51 cells were used as a control.

Finally, we investigated the mechanism of internalization by analyzing TEM images of MDA-MB-468 cells (Figure 6). At 15 min incubation of MNP−C11 with uPAR-positive cells, nanoparticles adhered to the cell membrane forming an invagination with concomitant recruitment of clathrin, which promoted its polymerization (Figure 6A), consistent with a recognition event mediated by a specific receptor. The clathrin-dependent mechanism of endocytosis was confirmed by the next observations at longer times of exposure, in which nanoparticles were confined inside clathrin-coated micro-vescicles (1 h, Figure 6B) that evolved into larger late endosomes and lysosomes (4 h, Figure 6C). Overall, the above steps of internalization represent strong evidence in support of the hypothesis of an uptake triggered by a receptor-mediated endocytosis.

CONCLUSIONS

In summary, we have developed a new conjugation strategy based on the "bimodular ligation" approach to control the protein positioning on multifunctional nanoparticles. Among the protein conjugation strategies adopted for colloidal nanoparticles, this method, involving the use of capture-protein domains in fusion with homing peptides,[20,21] has been established once again toward the specific targeting of a known cancer cell membrane receptor, urokinase Plasminogen Activator Receptor (uPAR). Our method takes advantage of the recombinant DNA technology to suitably modify the protein sequence of an ordinary esterase, namely, cutinase, which can act as a capture module to mediate the immobilization of an 11-amino-acid short peptide (U11) on the surface of nanoparticles. The functionalized nanoparticles proved to be efficient and selective in targeting uPAR-positive breast cancer cells. The resulting MNP covalently bound with CUT−U11 has potential as a modular delivery platform with "nano" dimension for active targeting or as an imaging probe. In principle, this versatile method offers an elegant solution for the covalent conjugation of a selection of homing ligands on the surface of nanoparticles, which could be directed toward a broad variety of specific cancer cell biomarkers. For all these reasons, this approach can be considered of general value for the development of targeted nanoparticles for biomedical applications. Moreover, part of this work was focused on the investigation of the discrimination between specific and nonspecific protein immobilization, an important issue in the design and development of nanobioconjugates, which is often underestimated. In this context, we have found a useful strategy to better control CUT−U11 ligation with the possibility of estimating the amount of immobilized peptide. Further investigations on new methods devoted to improving the selectivity and directionality of protein binding to colloidal nanoparticles are ongoing.

EXPERIMENTAL PROCEDURES

Materials and Methods. All reagents and solvents were purchased from Sigma-Aldrich (St. Louis, MO) and used as received. Water was deionized and ultrafiltered by a Milli-Q apparatus from Millipore Corporation (Billerica, MA) before use. TEM images were obtained by a Zeiss EM-109 microscope operating at 80 kV, available at the "Centro di Microscopia Elettronica per le Nanotecnologie applicate alla medicina" (CMENA, University of Milan). Dynamic light scattering (DLS) measurements were performed at 90° with 90Plus Particle Size Analyzer from Brookhaven Instruments Corporation (Holtsville, NY), working at 15 mV of a solid-state laser (λ = 661 nm). The final sample concentration used for measurements was typically 0.045 mg mL^{-1}. The calculations of hydrodynamic diameter were performed according to Mie theory, considering absolute viscosity and refractive index values of the medium to be 0.911 cP and 1.334, respectively. Zeta potential measurements were elaborated on the same instrument equipped with AQ-809 electrode and dates were processed by *ZetaPlus* software. Viscosity and refractive index of pure water were used to characterize the solvent. The samples for measurements were prepared by diluting the nanoparticle in 1 mM NaCl solution, pH 7.0 phosphate buffer, to a final

DOI: 10.1021/acs.bioconjchem.5b00005
Bioconjugate Chem. 2015, 26, 680−689

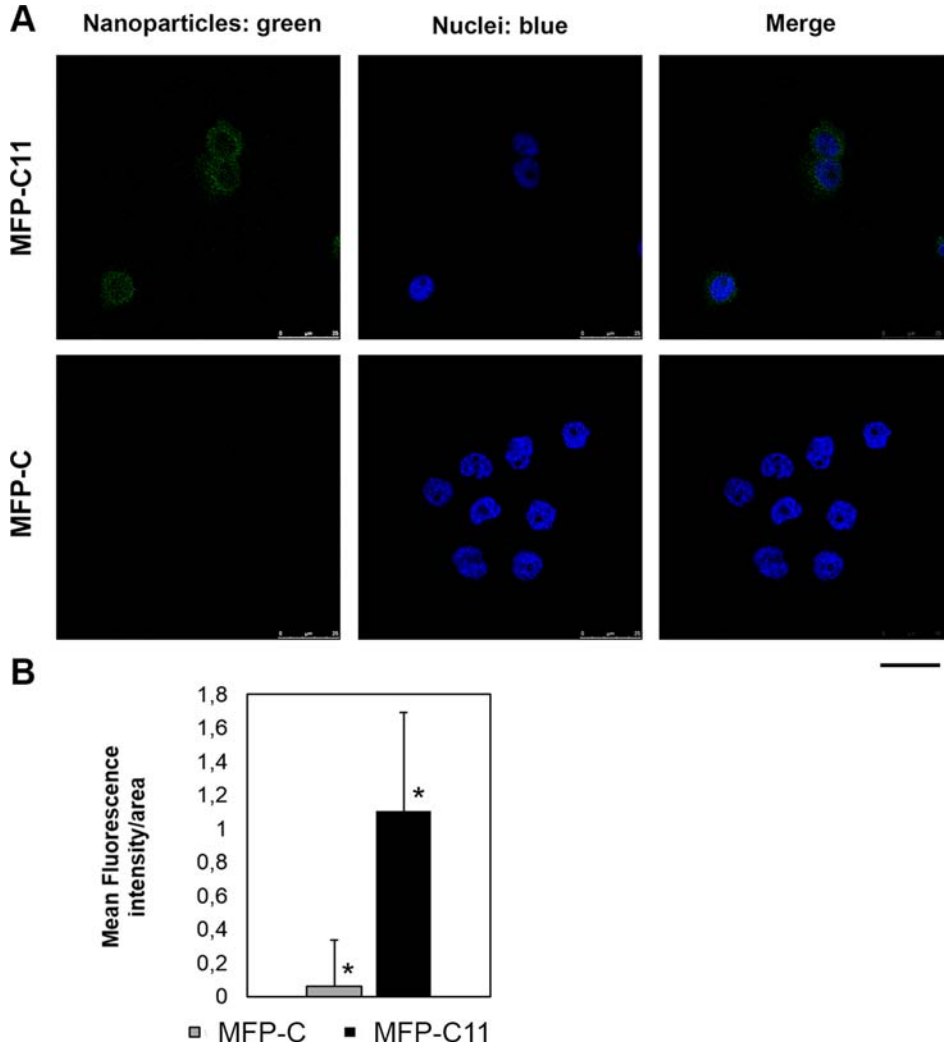

Figure 5. (A) Confocal microscopy images of MDA-MB-468 cells, incubated for 1 h at 37 °C with MFP−C11 and MFP−C (100 μg mL^{-1}). Nuclei were stained with 4′,6-diamidino-2-phenyl-indole (DAPI). Scale bar: 25 μm. (B) Quantification of fluorescence intensity due to MFP. Reported values obtained with *ImageJ* software represent the mean fluorescence intensity of 100 cells from six different images ± standard error. * $P < 0.05$. Autofluorescence from untreated cells was subtracted.

concentration of 10 μg mL^{-1}. A minimum of three runs and ten subruns per sample were performed to establish measurement reproducibility. The ζ-potential was processed by *ZetaPlus* software (Brookhaven Instrument Corporation, Holtsville, NY), considering a viscosity of 0.891 cP and a dielectric constant of 78.6 for the medium. Nanoparticles were dispersed in the solvent and sonicated in a S15H Elmasonic apparatus (Elma, Singen, Germany) before analysis. UV−vis spectra were recorded using a Nanodrop 2000C spectrophotometer (Thermo Fisher Scientific, Wilmington, Germany) in an absorbance range between 200 and 700 nm. Fluorescence measurements were performed with FluoroMax-4 Spectrofluorometer (Horiba Scientific, Edison, NJ), using Hellma fluorescence Suprasil cuvette quartz with pathlength of 1 mm; nanoparticles were dispersed in water and analyzed at a final concentration of 10 μg mL^{-1}.

Procedure of the Synthesis of Cutinase Linker (L1). L1 was prepared in a five-step synthesis starting from commercially available 11-Bromoundecanol.[34] The hydroxyl group was initially protected with 3,4-dihydro-2*H*-pyran and later reacted with diethyl phosphate. The relative undecylphosphonate was deprotected from the pyranoic derivative obtaining diethyl (11-hydroxyundecyl)phosphonate, which was reacted with 1,1-carbonyldiimidazole. The phosphonate moiety was mono-activated with oxalyl dichloride, which further reacted with *p*-nitrophenol in alkaline conditions, giving the desired substrate for cutinase reaction. The as-produced linker possessed the imidazole functional group for NP anchoring and the natural substrate for the enzymatic bioconjugation at the same time. A detailed description of the L1 synthetic route is available in the Supporting Information.

Synthesis of Surfactant-Coated Fe_3O_4 Nanoparticles (MNP0). Magnetic nanoparticles were synthesized according to Park et al.[31] At first, the iron oleate complex was prepared by reacting $FeCl_3 \times 6H_2O$ (2.7 g, 10 mmol) and sodium oleate (9.1 g, 30 mmol) in a reaction mixture containing ethanol (20 mL), distilled water (15 mL), and hexane (35 mL). The resulting biphasic solution was heated to 70 °C and kept under reflux for 4 h. At the end of the reaction, the upper organic layer containing the iron oleate complex was washed thrice with deionized water (25 mL) and once with brine (30 mL) in a separatory funnel. After washings, the organic phase was separated and filtered, and subsequently the hexane was evaporated off, resulting in the iron oleate complex in the

DOI: 10.1021/acs.bioconjchem.5b00005
Bioconjugate Chem. 2015, 26, 680−689

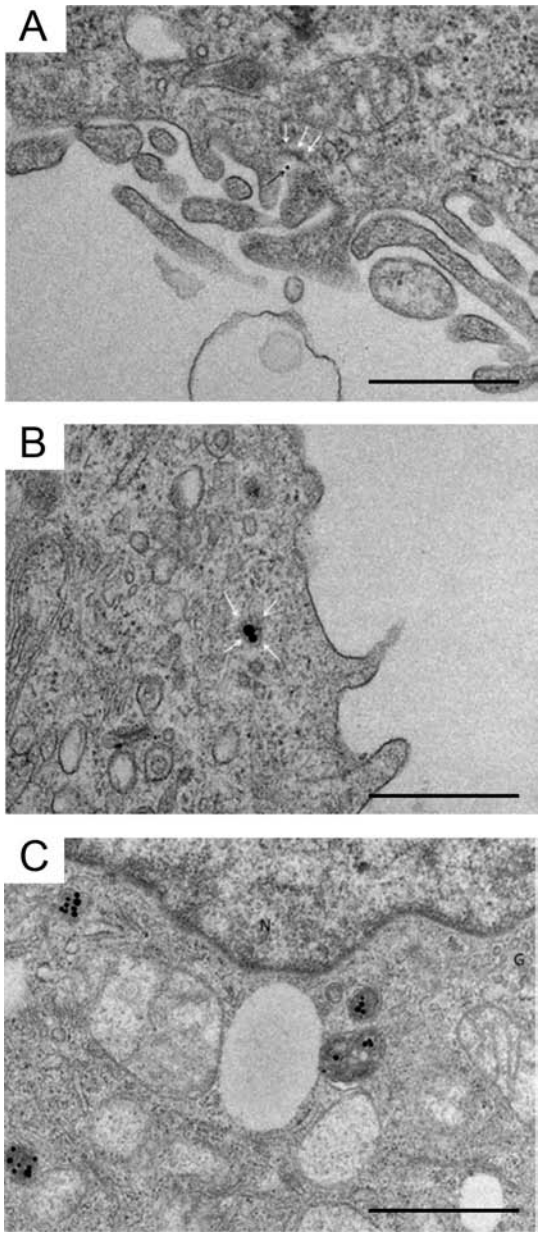

Figure 6. TEM images of uPAR-positive MDA-MB-468 cells exposed to 100 μg MNP−C11 after (A) 15 min, (B) 1 h, and (C) 4 h of incubation. Black arrow indicates MNP−C11 adjacent to the cell membrane; white arrows indicate the formation of clathrin superstructures; N = nucleus; G = Golgi apparatus. Scale bar = 500 nm.

form of a waxy dark red oil. Later on, Fe_3O_4 nanocrystals were synthesized by solvothermal decomposition of the iron oleate precursor. The complex (8 g, 8.9 mmol) and oleic acid (1.25 g, 4.5 mmol) were dissolved in 1-octadecene (57 mL) at room temperature. The reaction mixture was heated at 320 °C for 30 min. Then, the resulting black nanocrystal (NC) suspension was cooled to room temperature, and a mixture of ethanol−hexane 4:1 (100 mL) was added with the aim to sediment NCs by high-speed centrifugation (9000 *g*, 30 min). The Supernatant was discarded, and NCs were washed twice with ethanol−hexane 4:1 (100 mL) to remove unbound surfactants. The resulting oleic acid-coated magnetite NCs (called MNP0) were dispersed in chloroform ($CHCl_3$) (10 mg mL^{-1}) and stored at room temperature for further experiments.

Synthesis of Fluorescent PMA-Coated Fe_3O_4 Nanoparticles (MFP1). A 1.0 M fluoresceinamine solution in dimethyl sulfoxide (0.5 mL) was added to a 0.5 M poly(isobutylene-*alt*-maleic anhydride) polymer (PMA) solution in $CHCl_3$ (5 mL). The mixture was reacted overnight at room temperature under stirring. An aliquot of this solution (63 μL) was added to MNP0 (4.6 mg in $CHCl_3$) and the mixture was sonicated for 1 min; the solvent was then evaporated under reduced pressure. Sodium borate buffer (SBB) at pH 12 (10 mL) was added to redisperse all fluorescent polymer-coated NCs as an aqueous dispersion (called MFP1), which was concentrated in Amicon tubes (MW cutoff 100 kDa) by centrifugation (2000 *g*, 10 min). MFP1 were washed two times in water and finally concentrated to a final concentration of 5 mg mL^{-1}.

Synthesis of PMA-Coated Fe_3O_4 Nanoparticles Functionalized with (2,2-(Ethylendioxy)bisethylamine (MNP2 or MFP2). A 0.5 M PMA solution in $CHCl_3$ (63 μL) was added to MNP0 (4.6 mg in $CHCl_3$), and the mixture was treated as described above for fluorescent MFP1. The concentrated nanoparticle water suspension (5 mg mL^{-1}) (MNP1 or MFP1) was reacted with aqueous 0.1 M *N*-(3-(dimethylamino)propyl)-*N*′-ethylcarbodiimide hydrochloride (EDC•HCl) (18 μL) for 2 min. Then, aqueous 0.05 M (2,2-(ethylendioxy)bisethylamine (EDBE) (9 μL) was added and the suspension was reacted 2 h at room temperature, obtaining MNP2 or MFP2.

Synthesis of PMA-EDBE-Coated Fe_3O_4 Nanoparticles Functionalized with Cutinase Alkyl Phosphonate Substrate (MNP3 or MFP3). L1 was bound to MNP2 or MFP2 through amide coupling reaction with the primary amine of EDBE. L1 (800 μL) dissolved in dimethyl sulfoxide (10 mg mL^{-1}) was added to the same amount of MNP2 or MFN2. The water suspension was allowed to react overnight at 4 °C. The resulting functionalized MNP3 and/or MFP3 were washed with water, concentrated in Amicon tubes (5 mg mL^{-1}), and stored at 4 °C for protein conjugation.

CUT DNA Synthesis and Cloning in pET-11a Vector. A modified DNA sequence encoding for CUT and cloned in a pET-11a vector between *NdeI* and *Bam*HI restriction sites was a generous gift from Prof. M. Mrksich, University of Chicago. Plasmidic DNA (pET-11a/CUT) was sequenced and used to transform *E. coli* expression strain OrigamiB(DE3). A schematic representation of pET-11a/CUT vector is available in the supplementary file (see Figure S3).

CUT−U11 DNA Synthesis and Cloning in pET-30b(+) Vector. The DNA sequence encoding for CUT−U11 has been designed inserting the U11 peptide sequence (VSNKYFSNIHW) and the Ser−Gly spacer (GGGGSGGGG) in 5′ of cutinase DNA. Moreover, the restriction sites of *NdeI* and *BglIII* were inserted at 5′ and 3′ positions, respectively. The resulting CUT−U11 DNA sequence was synthesized and cloned in a pET-30b(+) vector between *NdeI* and *BglIII* restriction sites by Eurofins MWG Operon (Ebersberg) obtaining CUT−U11 sequence fused with His-Tag. Plasmidic DNA (pET-30b/CUT−U11) was sequenced and used to transform *E. coli* expression strain Tuner(DE3): F^-*ompT* $hsdS_B$ (r_B^- m_B^-) *gal dcm lacY1*. A schematic representation of pET-30b/CUT-U11 vector is available in the Supporting Information (see Figure S6).

CUT Expression and Purification. *E. coli* strain Origami-(DE3)/pET-11a/CUT was grown at 37 °C in LB-ampicillin medium until they reached A_{600} = 1 nm under stirring and

DOI: 10.1021/acs.bioconjchem.5b00005
Bioconjugate Chem. 2015, 26, 680−689

induced overnight with 1 mM IPTG at 18 °C with the yield of 3.3 g of cells L^{-1} of culture. The crude extract was prepared resuspending cells in lysis buffer (5 mL g^{-1} wet weight: 50 mM Na_2HPO_4, 300 mM NaCl pH 7.4, 100 mM $MgCl_2$, 10 mM imidazole). Lysozyme (1 mg mL^{-1}), DNaseI (0.2 mg g^{-1} cells, wet weight), and 1% Triton X-100 were added to cell suspension, and the sample was incubated for 30 min RT and sonicated. Finally, it was centrifuged for 30 min at 18000 *g*, 4 °C. The supernatant was loaded onto His-pure-cobalt resin (1 mL bed volume, Thermo Scientific, Rockford, Illinois, USA) pre-equilibrated with 10 volumes of equilibration buffer (50 mM Na_2HPO_4/300 mM NaCl pH 7.4, 10 mM imidazole). Then, it was washed with 10 volumes of equilibration buffer. CUT was eluted in 4 fraction of 2 mL each with a stepwise gradient of imidazole (from 50 mM to 200 mM). Eluted fractions were then analyzed by SDS−PAGE and Western blot. SDS-PAGE was performed according to Laemmli using 12% (v/v) polyacrylamide gels (Figure S4). The proteins were labeled by Gel Code Blue Stain Reagent (Pierce, Rockford, Illinois, USA) staining. Protein content was assessed with Bradford assay. Western blot analysis was performed using an His-probe specific the His-tag fused at the C-terminus of the protein (Figure S5).

CUT−U11 Expression and Purification. *E. coli* strain Tuner(DE3)/pET-30b/CUT−U11 was grown at 37 °C in LB-kanamicin medium until they reached A_{600} = 1 nm under stirring and induced 3 h with 0.05 mM IPTG, with the yield of 4.6 g of cells L^{-1} of culture. The crude extract was prepared resuspending cells in lysis buffer (3 mL g^{-1} wet weight: 50 mM Na_2HPO_4/300 mM NaCl, pH 8.0, 0.5 mM phenylmethanesulfonyl fluoride, protease inhibitor). Lysozyme (1 mg mL^{-1}), DNaseI (0.2 mg g^{-1} cells, wet weight), and 1% Triton X-100 were added to cell suspension, and the sample was incubated for 30 min RT and sonicated. Finally, it was centrifuged for 30 min at 18000 *g*, 4 °C. The supernatant was loaded onto Ni−NTA Superflow resin (0.5 mL bed volume, Quiagen S.p.a., Milan, Italy) pre-equilibrated with 10 volumes of equilibration buffer (50 mM Na_2HPO_4/300 mM NaCl pH 8). Then, it was washed with 10 volumes of equilibration buffer. CUT−U11 was eluted in 5 fractions with a stepwise gradient of imidazole (from 100 mM to 300 mM). Eluted fractions were then analyzed by SDS−PAGE and Western blot. SDS−PAGE was performed according to Laemmli using 12% (v/v) polyacrylamide gels (Figure S7). The proteins were determined by Gel Code Blue Stain Reagent (Pierce, Rockford, Illinois, USA) staining. Protein content was assessed with Bradford assay. Western blot analysis was performed using an anti His-tag monoclonal antibody specific the His-tag fused at the C-terminus of the protein (Figure S8).

CUT and CUT−U11 Labeling. CUT and CUT−U11 were labeled by incubating CUT−U11 (1 mg mL^{-1}, 1 mg) in 0.1 M sodium carbonate-bicarbonate buffer at pH 8.9 with fluoresceine isothiocyanate (2 mg) (Sigma) overnight at 4 °C. CUT−F and CUT−U11−F were purified from unreacted FITC through Sephadex G-25 M column. Protein absorbance was measured using Nanodrop 2000*c*/2000 UV−vis spectrophotometers (Thermo Scientific), and determined using *Protein and labels* software.

Activity Assay. The enzymatic activity of CUT and CUT−U11 was measured spectrophotometrically based on the ability of the enzyme to hydrolyze its substrate, 4-nitrophenyl decanoate, and produce the chromogenic product 4-nitrophenol (extinction coefficient ε = 17 mM^{-1} cm^{-1}, λ = 420 nm). The assay was performed monitoring the absorbance increase at 420 nm for 10 min, RT (25 °C). Five micrograms of the enzyme was added to a mix of 4-nitrophenyl decanoate 10 mM in isopropanol (0.02 mL) and Tris-HCl 100 mM, arabic gum 0.1%, and Triton X-100 0.02% (1.98 mL) in a final volume of 2 mL. A cuvette without the enzyme was used as a blank.

Inhibition Assay. The inhibition of CUT and CUT−U11 was carried out adding 4-nitrophenyl phosphonate as inhibitor at three different concentrations (0.5 μM, 5 μM, 10 μM). Enzyme (10 μg) was incubated in 100 mM Tris-HCl, 0.1% arabic gum, and 0.02% Triton X-100 (1.96 mL). 4-Nitrophenyldecanoate at the indicated final concentrations was added. The decrease of enzymatic activity was measured by monitoring the decrease of absorbance at 420 nm, RT (25 °C).

Synthesis of MNP−C and MNP−C11. MNP3 (125 μg) was incubated 1 h at room temperature under gentle stirring with CUT−FITC (250 μg) or CUT−U11−FITC (250 μg) in PBS pH 7.2 supplemented with BSA 0.3 wt %. Unconjugated protein was removed by centrifugation of the sample with Amicon YM-100. MNP−C and MNP−C11 were washed three times in Amicon YM-100 using PBS buffer. The amount of immobilized protein on nanoparticles was determined by measuring fluorescence emission of the sample exciting at 488 nm, using the standard calibration curve (Figure S10).

Synthesis of MFP−C and MFP−C11. MFP3 (125 μg) was incubated 1 h at room temperature under gentle stirring with CUT (250 μg) or CUT−U11 (250 μg) in PBS pH 7.2 supplemented with BSA 0.3 wt %. Unconjugated protein was removed by centrifugation of the sample with Amicon YM-100. MFP−C and MFP−C11 were washed three times in Amicon YM-100 using PBS buffer. The amount of immobilized protein on nanoparticles was determined by subtracting the amount of protein collected in the three washes obtained by Amicon centrifugations (Table S4), to the initial 250 μg incubated. All measurements were performed by Bradford assay.

Cell Cultures. MDA-MB-468 (uPAR-positive) and CAL-51 (uPAR-negative) human breast cancer cells were cultured in DMEM high glucose supplemented with 10% fetal bovine serum, L-glutamine (2 mM), penicillin (50 UI mL^{-1}), and streptomycin (50 mg mL^{-1}) at 37 °C and 5% CO_2 in a humidified atmosphere and subcultured prior to confluence using trypsin/EDTA. Cell culture medium and chemicals were purchased from EuroClone.

Confocal Laser Scanning Microscopy. MDA-MB-468 cells were cultured on collagen (Sigma) precoated coverglass slides until 90% confluence and incubated for 1 h at 37 °C with 100 μg of MFP−C11 or MFP−C. Treated cells were washed with PBS, fixed for 10 min with 4% paraformaldehyde (Sigma), and then treated for 10 min with 0.1 M glycine (Sigma) in PBS. A blocking step was performed for 1 h at room temperature with a solution containing 2% bovine serum albumin (Sigma), 2% goat serum, and DAPI (4′,6-diamidino-2-phenylindole, Invitrogen) at 0.2 μg mL^{-1} in PBS. Microscopy analyses were performed with a Leica SPE AOBs microscope confocal system. Images were acquired with 63× magnification oil immersion lenses at 1024 × 1024 pixel resolution. The quantification of the fluorescence intensity due to MFP−C or to MFP−C11 was performed on 100 cells from six different images using *ImageJ* software applied to the relevant sample images.

Transmission Electron Microscopy (TEM). MDA-MB-468 cells were incubated for 15 min, 1 h, and 4 h with 100 μg of MNP−C11. After incubation, cell pellets were washed in PBS (5 min, twice), fixed in 2.5% glutaraldehyde (Electron

DOI: 10.1021/acs.bioconjchem.5b00005
Bioconjugate Chem. 2015, 26, 680−689

Microscopy Sciences), 0.1 M phosphate buffer, pH 7.2, for 2 h. After one rinse with PBS, specimens were postfixed in 1.5% OsO_4 (Electron Microscopy Sciences) for 2 h. Then, they were dehydrated by 70%, 90%, and 100% EtOH, and embedded in epoxy resin (PolyBed 812 Polysciences Inc. USA). Ultrathin sections were stained with uranyl acetate and lead citrate and further examined by means of TEM (FEI, Tecnai Spirit).

■ ASSOCIATED CONTENT

Supporting Information

The complete chemical synthesis of L1, CUT, and CUT−U11 biochemical engineering, nanoparticle characterization and colloidal stability, protein−nanoparticle conjugate analyses by fluorescence spectroscopy, supplementary tables, and BSA-coated nanoparticle interaction with cells. This material is available free of charge via the Internet at http://pubs.acs.org.

■ AUTHOR INFORMATION

Corresponding Authors

*E-mail: serena.mazzucchelli@gmail.com. Phone: +39 02 39044050.

*E-mail: davide.prosperi@unimib.it. Phone: +39 02 64483302. Fax: +39 02 64483565.

Author Contributions

Elisabetta Galbiati and Marco Cassani contributed equally.

Notes

The authors declare no competing financial interest.

■ ACKNOWLEDGMENTS

We acknowledge Prof. Milan Mrksich and the University of Chicago, Illinois, for kindly providing us with pCut22b plasmid. This work was supported by the Fondazione Regionale per la Ricerca Biomedica (FRRB), NanoMeDia Project (Regione Lombardia and "L. Sacco" Hospital) and Cariplo Foundation ("The MULAN program", Project No. 2011-2096).

■ REFERENCES

(1) Schroeder, A., Heller, D. A., Winslow, M. M., Dahlman, J. E., Pratt, G. W., Langer, R., Jacks, T., and Anderson, D. G. (2011) Treating metastatic cancer with nanotechnology. *Nat. Rev. Cancer 12*, 39−50.

(2) Yu, M. K., Park, J., and Jon, S. (2012) Targeting strategies for multifunctional nanoparticles in cancer imaging and therapy. *Theranostics 2*, 3−44.

(3) Huang, X., Peng, X., Wang, Y., Wang, Y., Shin, D. M., El-Sayed, M. A., and Nie, S. (2010) A reexamination of active and passive tumor targeting by using rod-shaped gold nanocrystals and covalently conjugated peptide ligands. *ACS Nano 4*, 5887−5896.

(4) Lewin, M., Carlesso, N., Tung, C.-H., Tang, X.-W., Cory, D., Scadden, D. T., and Weissleder, R. (2000) Tat peptide-derivatized magnetic nanoparticles allow in vivo tracking and recovery of progenitor cells. *Nat. Biotechnol. 18*, 410−414.

(5) Thanh, N. T. K., and Green, L. A. W. (2010) Functionalization of nanoparticles for biomedical applications. *Nano Today 5*, 213−230.

(6) Simberg, D., Duza, T., Park, J. H., Essler, M., Pilch, J., Zhang, L., Derfus, A. M., Yang, M., Hoffman, R. M., Bathia, S., et al. (2010) Biomimetic amplification of nanoparticle homing to tumors. *Proc. Natl. Acad. Sci. U.S.A. 104*, 932−936.

(7) Algar, W. R., Prasuhn, D. E., Stewart, M. H., Jennings, T. L., Blanco-Canosa, J. B., Dawson, P. E., and Medintz, I. L. (2011) The controlled display of biomolecules on nanoparticles: a challenge suited to bioorthogonal chemistry. *Bioconjugate Chem. 22*, 825−858.

(8) Medintz, I. (2006) Universal tools for biomolecular attachment to surfaces. *Nat. Mater. 5*, 842.

(9) Sapsford, K. E., Algar, W. R., Berti, L., Gemmill, K. B., Casey, B. J., Oh, E., Stewart, M. H., and Medintz, I. L. (2012) Functionalizing nanoparticles with biological molecules: developing chemistries that facilitate nanotechnology. *Chem. Rev. 113*, 1904−2074.

(10) Avvakumova, S., Colombo, M., Tortora, P., and Prosperi, D. (2014) Biotechnological approaches toward nanoparticle biofunctionalization. *Trends Biotechnol. 32*, 11−20.

(11) Haun, J. B., Devaraj, N. K., Hilderbrand, S. A., Lee, H., and Weissleder, R. (2010) Bioorthogonal chemistry amplifies nanoparticle binding and enhances the sensitivity of cell detection. *Nat. Nanotechnol. 5*, 660−665.

(12) Mazzucchelli, S., Colombo, M., De Palma, C., Salvadè, A., Verderio, P., Coghi, M. D., Clementi, E., Tortora, P., Corsi, F., and Prosperi, D. (2010) Single-domain protein A-engineered magnetic nanoparticles: toward a universal strategy to site-specific labeling of antibodies for targeted detection of tumor cells. *ACS Nano 4*, 5693−5702.

(13) Montenegro, J. M., Grazu, V., Sukhanova, A., Agarwal, S., de la Fuente, J. M., Nabiev, I., Greiner, A., and Parak, W. J. (2013) Controlled antibody/(bio-) conjugation of inorganic nanoparticles for targeted delivery. *Adv. Drug Delivery Rev. 65*, 677−688.

(14) Park, K., Lee, S., Kang, E., Kim, K., Choi, K., and Kwon, I. C. (2009) New generation of multifunctional nanoparticles for cancer imaging and therapy. *Adv. Funct. Mater. 19*, 1553−1566.

(15) Lee, J.-H., Huh, Y.-M., Jun, Y.-W., Seo, J.-W., Jang, J.-T., Song, H.-T., Kim, S., Cho, E.-J., Yoon, H.-G., Suh, J.-S., et al. (2006) Artificially engineered magnetic nanoparticles for ultra-sensitive molecular imaging. *Nat. Med. 13*, 95−99.

(16) Kim, J., Park, S., Lee, J. E., Jin, S. M., Lee, J. H., Lee, I. S., Yang, I., Kim, J.-S., Kim, S. K., Cho, M.-H., et al. (2006) Designed fabrication of multifunctional magnetic gold nanoshells and their application to magnetic resonance imaging and photothermal therapy. *Angew. Chem., Int. Ed. 45*, 7754−7758.

(17) Corsi, F., Fiandra, L., De Palma, C., Colombo, M., Mazzucchelli, S., Verderio, P., Allevi, R., Tosoni, A., Nebuloni, M., Clementi, E., et al. (2011) HER2 expression in breast cancer cells is downregulated upon active targeting by antibody-engineered multifunctional nanoparticles in mice. *ACS Nano 5*, 6383−6393.

(18) Xu, C., Xu, K., Gu, H., Zhong, X., Guo, Z., Zheng, R., Zhang, X., and Xu, B. (2004) Nitrilotriacetic acid-modified magnetic nanoparticles as a general agent to bind histidine-tagged proteins. *J. Am. Chem. Soc. 126*, 3392−3393.

(19) Long, M. J. C., Pan, Y., Lin, H. C., Hedstrom, L., and Xu, B. (2011) Cell compatible trimethoprim-decorated iron oxide nanoparticles bind dihydrofolate reductase for magnetically modulating focal adhesion of mammalian cells. *J. Am. Chem. Soc. 133*, 10006−10009.

(20) Colombo, M., Mazzucchelli, S., Montenegro, J. M., Galbiati, E., Corsi, F., Parak, W. J., and Prosperi, D. (2012) Protein oriented ligation on nanoparticles exploiting O_6-alkylguanine-DNA transferase (SNAP) genetically encoded fusion. *Small 8*, 1492−1497.

(21) Mazzucchelli, S., Colombo, M., Verderio, P., Rozek, E., Andreata, F., Galbiati, E., Tortora, P., Corsi, F., and Prosperi, D. (2013) Orientation-controlled conjugation of haloalkane dehalogenase fused homing peptides to multifunctional nanoparticles for the specific recognition of cancer cells. *Angew. Chem., Int. Ed. 52*, 3121−3125.

(22) Hodneland, C. D., Lee, Y. S., Min, D. H., and Mrksich, M. (2002) Selective immobilization of proteins to self-assembled monolayers presenting active site-directed capture ligands. *Proc. Natl. Acad. Sci. U.S.A. 99*, 5048−5052.

(23) García, I., Gallo, J., Genicio, N., Padro, D., and Penadés, S. (2011) Magnetic glyconanoparticles as a versatile platform for selective immunolabeling and imaging of cells. *Bioconjugate Chem. 22*, 264−273.

(24) Los, G. V., Encell, L. P., McDougall, M. G., Hartzell, D. D., Karassina, N., Zimprich, C., Wood, M. G., Learish, R., Ohana, R. F., Urh, M., et al. (2008) HaloTag: a novel protein labeling technology for cell imaging and protein analysis. *ACS Chem. Biol. 3*, 373−382.

DOI: 10.1021/acs.bioconjchem.5b00005
Bioconjugate Chem. 2015, 26, 680−689

(25) Wang, M., Miller, A. D., and Thanou, M. (2013) Effect of surface charge and ligand organization on the specific cell-uptake of uPAR-targeted nanoparticles. *J. Drug Targeting 21*, 684−692.
(26) Quai, Q., Mazar, A. P., Quo, A., Parry, G. C., Shaw, D. E., Callahan, J., Li, Y., Yuan, C., Bian, C., Chen, L., et al. (2006) Structure of human urokinase plasminogen activator in complex with its receptor. *Science 311*, 656−659.
(27) LeBeau, A. M., Duriseti, S., Murphy, S. T., Pepin, F., Hann, B., Gray, J. W., Van Brocklin, H. F., and Craik, C. S. (2013) Targeting uPAR with antagonistic recombinant human antibodies in aggressive breast cancer. *Cancer Res. 73*, 2070−2081.
(28) Wang, M., Löwik, D. W. P. M., Miller, A. D., and Thanou, M. (2009) Targeting the urokinase plasminogen activator receptor with synthetic self-assembly nanoparticles. *Bioconjugate Chem. 20*, 32−40.
(29) Carvalho, C. M. L., Aires-Barros, M. R., and Cabral, J. M. S. (1998) Cutinase structure, function and biocatalytic applications. *Electr. J. Biotechnol. 15*, 160−173.
(30) Carvalho, C. M. L., Aires-Barros, M. R., and Cabral, J. M. S. (1999) Cutinase: from molecular level to bioprocess development. *Biotechnol. Bioeng. 66*, 17−34.
(31) Park, J., An, K., Hwang, Y., Park, J. G., Noh, H. J., Kim, J. Y., Park, J. H., Hwang, N. M., and Hyeon, T. (2004) Ultra-large-scale synthesis of monodisperse nanocrystals. *Nat. Mater. 3*, 891−895.
(32) Pellegrino, T., Manna, L., Kudera, S., Liedl, T., Koktysh, D., Rogach, A. L., Keller, S., Radler, J., Natile, G., and Parak, W. J. (2004) Hydrophobic nanocrystals coated with an amphiphilic polymer shell: A general route to water soluble nanocrystals. *Nano Lett. 4*, 703−707.
(33) Lin, C. J., Sperling, R. A., Li, J. K., Yang, T. Y., Lin, P. Y., Zanella, M., Chang, W. H., and Parak, W. J. (2008) Design of an amphiphilic polymer for nanoparticle coating and functionalization. *Small 4*, 334−341.
(34) Reetz, M. T., Rüggeberg, C. J., Dröge, M. J., and Qwax, W. J. (2002) The controlled display of biomolecules on nanoparticles: a challenge suited to bioorthogonal chemistry. *Tetrahedron 58*, 8465−8473.

DOI: 10.1021/acs.bioconjchem.5b00005
Bioconjugate Chem. 2015, 26, 680−689